Chapter 2. 2D thermohaline approach: model scenario and preliminary simulations

In this chapter the available NEGB structural model (Scheck 1997) will be integrated in the FEFLOW database. Then a representative cross-section of the basin will be obtained from this three dimensional structural model and used as model scenario for the 2D thermohaline simulations. In order to approach numerical simulations of coupled fluid flow, mass and heat transfer, based on the NEGB, a proper grid resolution has to be defined. The preliminary numerical simulations described here are aimed to build up a finite element mesh suitable for the thermohaline problem.

2.1 Definition of the two-dimensional model scenario for thermohaline simulations by use of FEFLOW®

2.1.1 The need of a two-dimensional approach

The basic problems in solving the coupled non-linear equations of fluid flow, heat and mass transport are due to numerical instabilities which arise during the simulation process. Numerical thermohaline simulations based on real geothermal systems are hindered by the highly deformed mesh geometry resulting from the complex geological structure. Consequently, a certain degree of mesh refinement is required in order to solve the density-dependent problems (Gresho and Sani 2000; Diersch and Kolditz 2002). However, mesh refinement increases the numerical complexity of the problem. Moreover, the different spatially varying physical parameters involved in the equations, provide additional difficulties in solving the thermohaline flow problem. Transport phenomena in sedimentary basin are controlled by the spatial variation in heterogeneous conductivity fields (Dagan 1989). As discussed by Simmons et al. (2001) heterogeneity of hydraulic properties can even perturb flow over regional length scales and generate instabilities especially in systems where density stratifications are encountered. These considerations summarize the major drawbacks concerning the numerical approach for thermohaline flow in geothermal system. In summary, from a numerical point of view, the complicated geometry of the basin fill, together with the

heterogeneity of physical parameters, and fluid density variations lead to self-perturbing natural systems.

Although fluid flow and transport processes in sedimentary basins occur in a three-dimensional environment, the study of a two-dimensional thermohaline problem is necessary in order to obtain more details with regard to numerical features of the non-linear coupled system. In a vertical profile (**x**,**z**) the number of independent spatial variables of the problem is reduced by one degree of freedom. Therefore a highly refined mesh can be defined in a cross-section model scenario by use of much less active nodes. Consequently the computational time decreases drastically. This allows to estimate a proper cell dimension for thermohaline flow simulation. Once the model robustness is achieved it is possible to define proper boundary conditions in order to reproduce observed data.

Therefore, the 2D approach provides a series of advantages in successfully tracking down a simulation-based method for developing stable solutions with regard to the given geometrical (structural) resolution, the physical equations and the numerical approximation. The method then can be used to tackle a three-dimensional thermohaline model scenario.

In order to create a cross section of the NEGB, with all spatial and physical characteristics preserved, the three-dimensional structural model of the basin had to be integrated into FEFLOW.

2.1.2 Integration of the structural model of the NEGB into FEFLOW©

FEFLOW is a software conceived for the modelling of flow and/or transport processes in natural porous media. FEFLOW has been chosen for this study for several reasons. The code is based on the Finite Element technique and it is one of the few commercial softwares which can handle two-dimensional and three-dimensional thermohaline flow. The finite element method is suitable for defining grids which can be easily adapted to the complicated structure of a sedimentary basin such as the NEGB. Moreover FEFLOW offers a Geographic Information System interface (GIS) whereby data integration and regionalization can be applied. These components ensure an efficient working tool in building the finite element mesh, integrating structural model data, and assigning model properties.

The first step for building the numerical model scenario is to define a so called superelement. The superelement delimits the horizontal extension (**x**,**y** direction) of the 3D finite element mesh within the working window of FEFLOW. For constructing the finite element mesh, the grid resolution has to be defined within the superelement. The discretized

superelement is also referred to as a slice. Once the slice is built, it is possible to integrate the geometrical characteristics of the different stratigraphic units of the NEGB in FEFLOW's database. A layer, i.e. a stratigraphic unit, is composed of two slices also referred to as top and bottom slices. In order to define a layer, the z-coordinate (or elevation) of each node of the top and bottom slices must be assigned. Therefore the layer resolution is determined by the finite element grid resolution in the horizontal and by the layer thickness in the vertical direction. The structural model of the NEGB was incorporated in FEFLOW by applying the described procedure for each model slice.

As mentioned in paragraph 1.2.2, the study area covers a rectangular surface of 230 x 330 km. Therefore the chosen superelement is a rectangle, in which the corner coordinates have been referred to the Gauss-Krueger coordinates of the NEGB. The finite element resolution constructed in this superelement is identical with the grid resolution of the structural model (Scheck 1997). Hence each model slice consists of 60 x 70 grid points (or nodes) in the West-East and North-South direction respectively. Consequently the mesh resolution of a layer is approximately 3.9 x 4.8 km in the horizontal direction while in the vertical direction the discretization results from layer thickness which is strongly variable. At this resolution the structure and geometry related to the NEGB stratigraphic units are accurately preserved in FEFLOW database. Fig. 2-1 is a 3D rendering illustrating the stratigraphic units incorporated in FEFLOW as well as the defined finite element mesh.

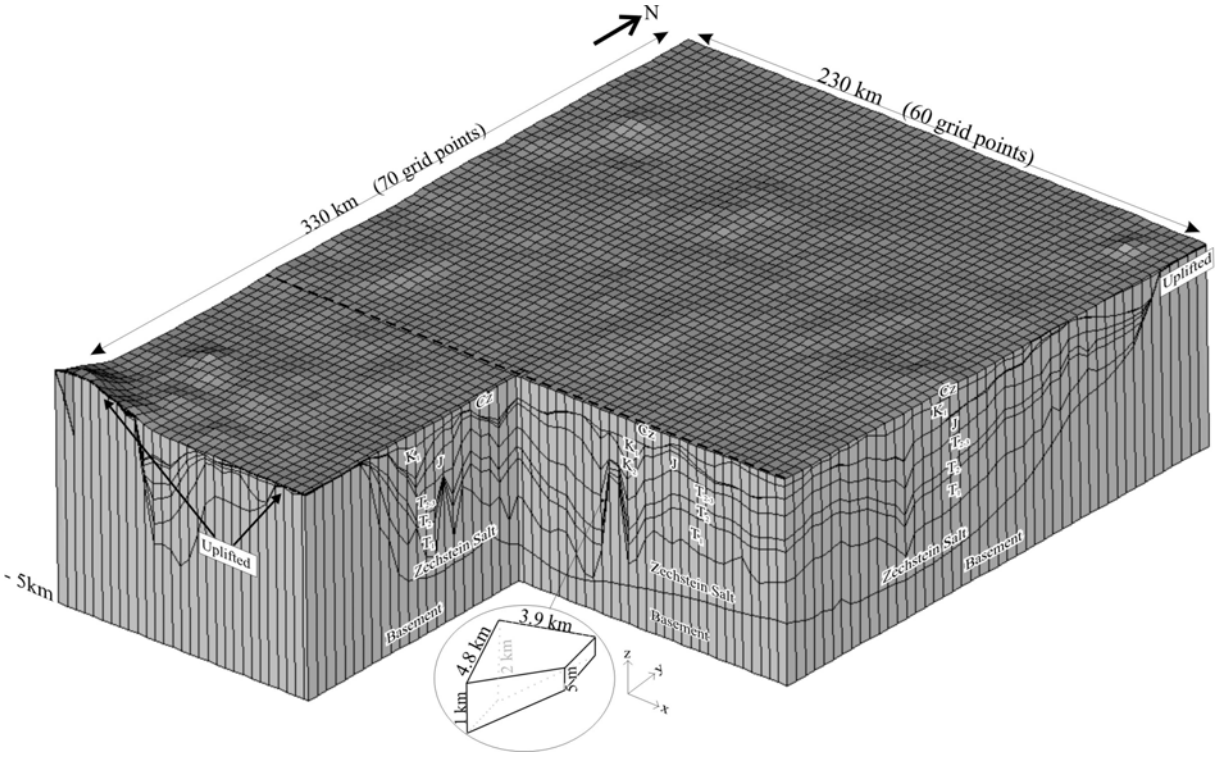

Fig. 2-1: 3D rendering of the NEGB incorporated in FEFLOW. The stratigraphic units abbreviations are given in Tab. 1-1. A detail of a finite element used to discretize the whole model volume is shown in the circle. The dashed line localizes the cross-section chosen for the 2D thermohaline model scenario (Fig. 2-2).

The actually implemented model consists of the first eight layers of the given geological model (from Top Cenozoic down to the base Zechstein Salt) and of an additional slice located at 5 km depth, acting as the model basement. This picture emphasizes the highly complicated structure of the layers especially in salt domes and uplifted areas. In Fig. 2-1, the finite element mesh used to define the top slice of all layers is shown for the topography. Each model slice consists of 4071 (59 x 69) rectangular elements. The 3D finite elements used to discretize the whole basin volume are eight-nodes quadrilateral prisms. Since 9 layers have been incorporated, the total number of 3D finite elements is 36639 corresponding to 42000 active nodes. In Fig. 2-1 a sketch of a 3D finite element representing a salt dome area is depicted. In this particular setting, finite elements are highly distorted since the height of the elements can drastically vary within few kilometres.

The physical parameters of all stratigraphic units, given in Tab. 1-1, can be stored in the FEFLOW database by assigning each layer the related parameter value. At this point the available 3-D structural model of the NEGB and the physical parameters are fully adapted to the simulation program. Cross-section modelling scenarios can be created from the 3-D structural model simply by taking a vertical profile through the structural model along a surface line as depicted in Fig. 2-1. The resulting cross-section will comprise the finite element mesh as well as the different physical parameters of each layer. In the next paragraph the selected representative cross-section will be described.

2.1.3 The representative NEGB cross-section

Two-dimensional investigation of thermohaline flow in the NEGB basin requires the choice of a proper model scenario. Indeed, as mentioned in the previous chapter, in the NEBG there is some topographical variations and particular geological structures such as salt pillows and diapirs. At a regional scale, topographical variations induce regional flow that can enhance hydrodynamic mixing and affect solute transport in the shallow aquifer. The steep flanks of the salt diapirs can further induce gravitational driven flow, also referred to as non-Rayleigh convection (Bjorlykke et al. 1988). Moreover, because of the high thermal conductivity of salt diapirs the temperature fields can be strongly disturbed favouring thermally induced flow and salt dissolution (Evans and Nunn 1989). Therefore, topographical variations and salt-tectonic structures must be comprised in the cross-section in order to gain insights in their interaction with other fluid-dynamics, affecting solute transport within the basin. Additionally the vertical profile must cross areas where observed data, such as salty plumes and saline springs

are observed. A cross-section in which all these features are comprised can be considered as a "good" or representative 2D model scenario for the NEGB.

In Fig. 2-2 (a) the location of the cross-section is shown on the NEGB topography together with the salty groundwater distribution (Grube et al. 2000) and the observed saline springs (Schirrmeister 1996). From this figure it can be seen that the chosen cross section slices the study area along the whole West-East basin extent. The cross-section cuts the main regions where topographical variations arise as well as a wide area of salty groundwater plumes. Some of the observed saline springs are located along the profile. The cross section does not intersect the uplifted area delimited by the southern margin since this region corresponds to eroded layers where fluid flow and mass transport play a minor role.

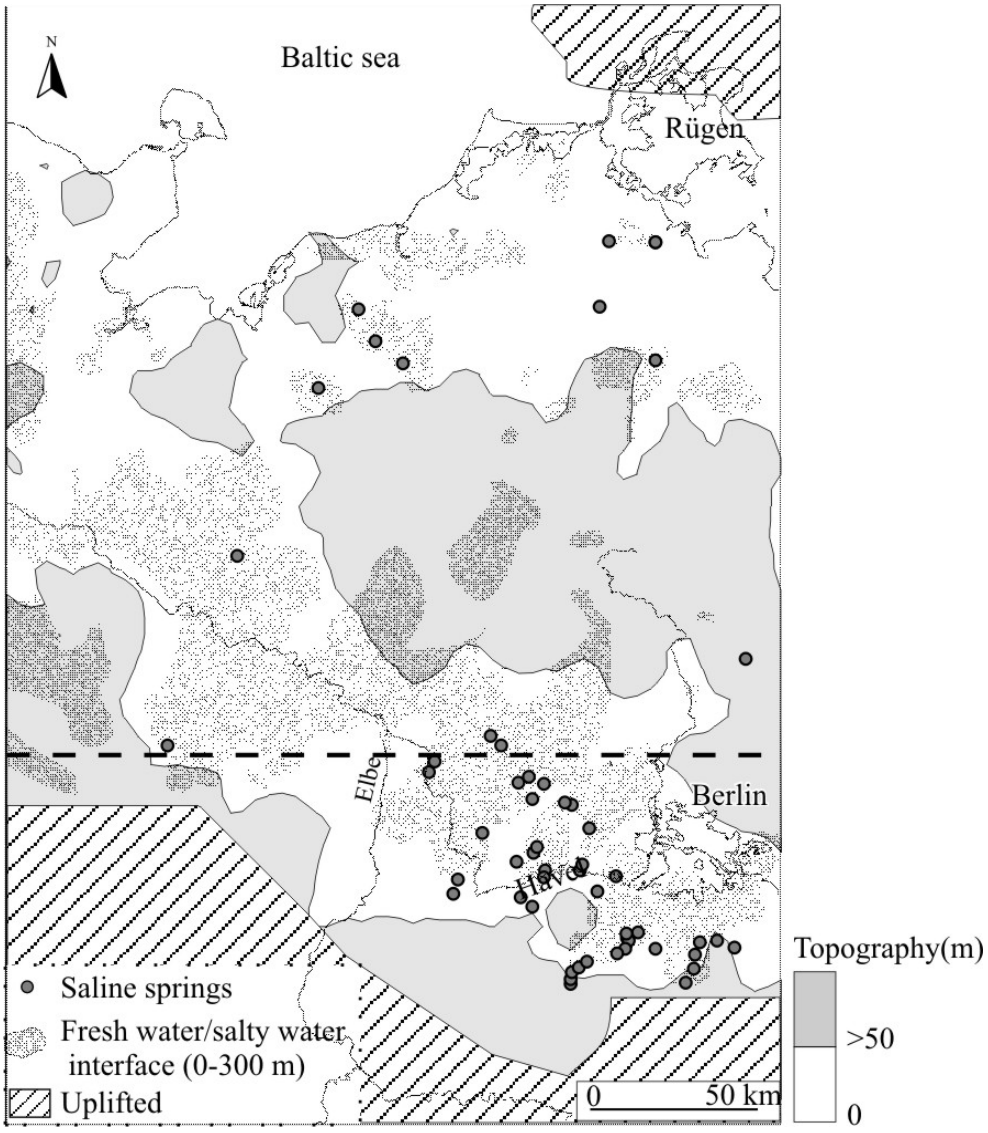

Fig. 2-2 a: Location of the 2D cross-section together with the fresh/salty water interface and saline springs as shown in Fig. 1-5

Fig. 2-2 (b) illustrates the geological structures of the chosen cross-section. Shallow salt-structures are comprised within the resulting profile area.

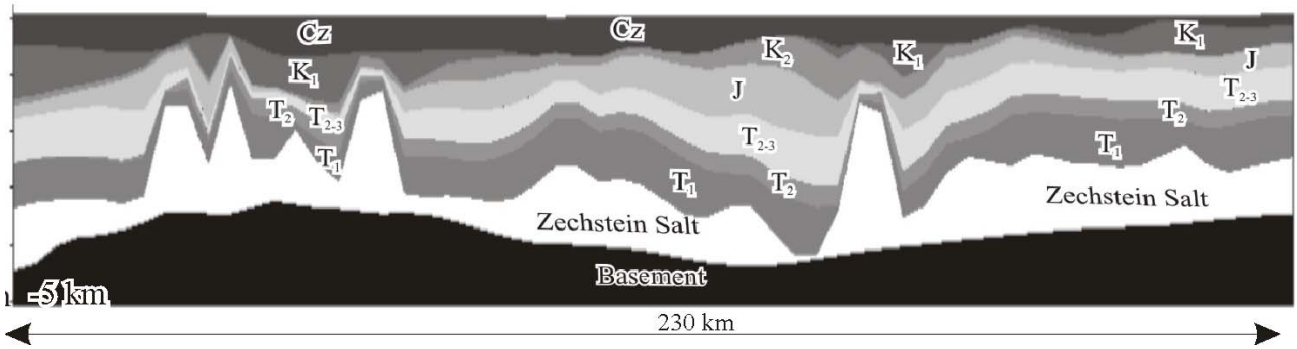

Fig. 2-2 b: Stratigraphic units of the 2D cross-section. The stratigraphic unit abbreviations are given in Tab. 1-1.

This cross section will be used as a representative model scenario for carrying out thermohaline simulations based on the NEGB as described in the next chapters. According to the geological features, the cross-section will allow to test and identify the different flow regimes within the NEGB (forced versus free convection). This purpose can be achieved only by use of a numerically stable solution. Therefore an adequate grid refinement will be essential in order to define a cell resolution which resolves short wavelength interactions of the coupled system. A robust 2D finite element mesh will be defined in the next paragraph by performing preliminary transient thermohaline simulations

2.2. Preliminary 2D thermohaline simulations

2.2.1. Governing equations and assumptions

The governing equations of thermohaline convection in a saturated porous media are derived from the conservation principles for linear momentum, mass and energy (e.g. Bear 1991; Kolditz et al. 1998; Nield and Bejan 1999). A description of the equations and parameters can be found in Appendix 1. The resulting system is fully implemented in FEFLOW and is briefly reported here by the following set of differential equations (ref. Appendix 1: Eq. 1.2; Eq. 1.5; Eq. 1.9; Eq. 1.16)

$$S_0 \frac{\partial \varphi}{\partial t} + \mathrm{div}(\mathbf{q}) = Q_{\mathrm{Boussinesq}} \tag{2.1}$$

$$\mathbf{q} = -\mathbf{K}\mathbf{grad}\left(\varphi + \frac{\rho_f - \rho_{0f}}{\rho_{0f}}\right) \tag{2.2}$$

$$\frac{\partial \phi C}{\partial t} + \mathrm{div}\left(\rho_f \mathbf{q} C\right) - \mathrm{div}\left(\mathbf{D}\mathbf{grad}(C)\right) = Q_C \tag{2.3}$$

$$\frac{\partial}{\partial t}\left(\left(\phi\rho_f c_f + (1-\phi)\rho_s c_s\right)T\right) + \mathrm{div}(\rho_f c_f T\mathbf{q}) - \mathrm{div}\left(\boldsymbol{\lambda}\mathbf{grad}(T)\right) = Q^T \tag{2.4}$$

Eq.(2.1) is the equation of fluid mass conservation. S_0 is the medium storativity which physically represents the volume of water released (or added to) from storage in the aquifer per unit volume of aquifer and per unit decline (or rise) of head φ. $Q_{\mathrm{Boussinesq}}$ is the Boussinesq term which incorporates first order derivatives of mass-dependent and temperature-dependent compression effects. $\mathbf{q}$ is the Darcy (or volumetric flux density) velocity defining the specific discharge of the fluid. The Darcy's law is expressed by Eq.(2.2) where $\mathbf{K}$ is the hydraulic conductivity tensor. Eq.(2.3) is the equation of solute mass conservation where ϕ is the porosity of the porous medium, C is the mass concentration, $\mathbf{D}$ is the tensor of hydrodynamic dispersion and Q^C is a mass supply. Eq.(2.4) is the energy balance equation of the fluid and the porous media. c_f and c_s is the heat capacity of the fluid and solid respectively, T is the temperature, $\boldsymbol{\lambda}$ is the thermal conductivity of the saturated porous medium as a whole.

From Eq.(2.1) and Eq.(2.2) it can be seen that FEFLOW uses a hydraulic head-formulation. This approach is usually preferred since it allows more convenient formulations of boundary conditions and parameters relations for shallow aquifers.

As mentioned in Appendix 1, constitutive and phenomenological relations of the different physical parameters involved in the equations are needed to close this coupled system. Here the hydraulic conductivity relation and the Equation Of State (EOS) for the fluid density are recalled (see Appendix 1 for details):

$$\mathbf{K} = \frac{\mathbf{k}\rho_{0f} g}{\mu_f(C,T)} \tag{2.5}$$

$$\rho^f = \rho_0^f \left(1 - \overline{\beta}(T,p)(T - T_0) + \overline{\gamma}(T,p)(p - p_0) + \frac{\overline{\alpha}}{C_s - C_0}(C - C_0)\right) \tag{2.6}$$

The hydraulic conductivity tensor $\mathbf{K}$ is related to the reference fluid density ρ_{0f}, g is the gravitational acceleration, $\mathbf{k}$ is the tensor of permeability, $\mu_f(C,T)$ takes into account the

fluid viscosity effects due to temperature and concentration variations. The EOS for the fluid density is related to the reference temperature T_0, pressure p_0 and concentration C_0, Eq.(2.6). $\bar{\alpha}$ is the mass concentration ratio, $\bar{\beta}$ is the coefficient of thermal expansion and. $\bar{\gamma}$ is the coefficient of compressibility.

The flow and transport equations (Eq.(2.2), Eq.(2.3), Eq.(2.4)) for thermohaline convection are non-linear and strongly coupled since temperature and salinity control the fluid density ρ^f and dynamic viscosity μ_f. The variation of fluid density is essential for the modelling of thermohaline convection because of its primary importance for calculating the correct buoyant force included in the equation of motion (i.e. generalized Darcy's law Eq.(2.2)). Fitted polynomial expressions are commonly used for temperature, pressure and salinity dependences of the fluid density (Sorey 1976). In order to reproduce the density model described in paragraph 1.2.3, all the mentioned dependences are accounted for FEFLOW. For this purpose, two polynomial expressions which accurately represents the coefficient of thermal expansion $\bar{\beta}(T, p)$ and compressibility $\bar{\gamma}(T, p)$ for the fluid density (Eq.(2.6)) have been derived and coded as an extension to the simulation program. A detailed description of these polynomial functions and the implemented code is reported in Appendix 2 and Appendix 3 respectively. The method has been approved by WASY and can also be found in Magri (2004). As seen in the paragraph 1.2.3, the density of the saturated brine is 1220g/L. The fluid density ρ_f^0 is referred to freshwater conditions and set equal to 1000 g/L. Therefore the density ratio $\bar{\alpha} = \frac{\rho^s{}_f - \rho^0{}_f}{\rho^0{}_f}$, appearing in Eq.(2.6), is set equal to 0.22.

Since the main goal of this chapter is the definition of a robust 2D finite element mesh a number of simplifying assumptions are required.

No coefficient of mechanical dispersion is included in the dispersive flux of the solute. This means that the coefficient of hydrodynamic dispersion **D** appearing in Eq.(2.3) is equal to the molecular diffusivity of solute in the saturated porous medium $\mathbf{D_{diff}}$ (Eq.(1.6) Appendix 1). In the specific case, such simplification may introduce differences in the resulting solute field (Nield 1974; Rubin 1975)). The mechanical dispersion takes into account the structure of the porous medium. As described in Appendix 1, the mechanical dispersion causes the flow streamlines to divide in the longitudinal direction. Consequently, this additional spreading enhances solute mixing with freshwater and the resulting fluid density differences become smoothed. Therefore, in the case where no coefficient of mechanical dispersion is considered

the solute field will be less homogenous and more saline. Nevertheless, as proved in Rosenberg and Spera (1992), neglecting the coefficient of mechanical dispersion does not affect the basic character of the fluid dynamics of the system. Therefore, this simplifying assumption will also be used for the thermohaline simulations described in the next chapter.

Another approximation which will be considered henceforth is the so called Oberdeck-Boussinesq approximation OB. The OB approximation consists in neglecting the density dependences included in the term $Q_{\text{Boussinesq}}$ in the LHS of the fluid balance equation (Eq.(2.1) and explicitly detailed in Eq.(1.43), Appendix 1), i.e. $Q_{\text{Boussinesq}} = 0$. Kolditz et al. (1998) evaluated the OB approximation for different convection problems. Their studies proved that the differences in the concentration field resulting from the OB approximation on a long term simulation are negligible and the fluid-dynamics is not affected.

Additionally, fluid viscosity is considered constant and referred to freshwater conditions. Viscosity effects on the flow regime will be evaluated only on a robust thermohaline model. In the next chapter the concentration and temperature dependences of viscosity will be incorporated in the thermohaline simulations. Other fluid properties such as heat capacity and conductivity are considered constant.

To complete the set of differential equations defining the thermohaline problem appropriate initial and boundary conditions for the hydraulic head, the temperature and the concentration must be defined.

2.2.2. Boundary and initial conditions

The boundary conditions used in this preliminary thermohaline approach are first and second type boundary conditions. A set of boundary conditions which can reproduce observed data such as mass and temperature distribution at the surface can be defined once a suitable grid for thermohaline flow is built. The boundary conditions used here are schematically illustrated as follows (Fig. 2-3 A.):

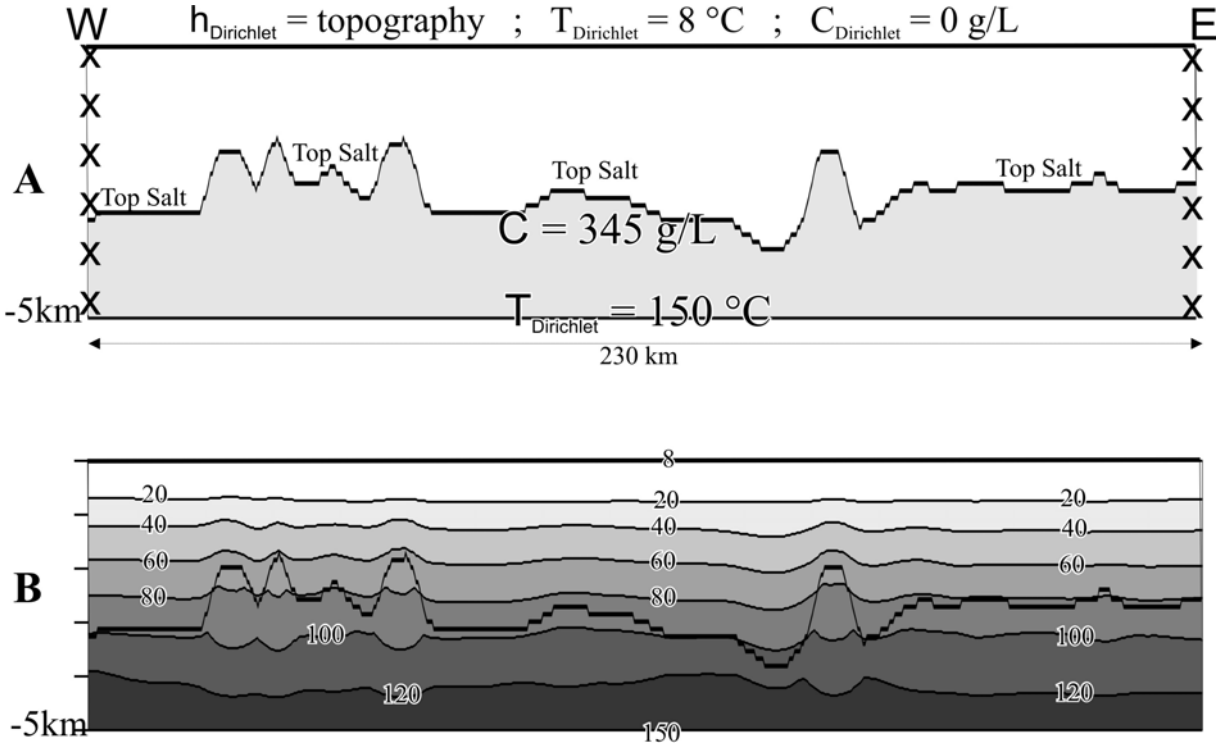

Fig.2-3: **A**: Boundary conditions of the preliminary thermohaline simulations and, **B**: Initial temperature distribution (°C) derived from a steady-state heat transport problem. The bold line delimits the Top Salt. Temperature values have been interpolated with a Kriging gridding method by use of the commercial software Surfer 8.

- At the surface the hydraulic head, fluid temperature and concentration have to be defined. The head is set equal to the topographical elevation. The fluid temperature and concentration values are fixed to 8°C and 0 g/L respectively.
- At the Top Salt a fixed concentration value of 345.2 g/L has been set. As seen in the paragraph 1.2.3 this value corresponds to the saturation concentration of the fluid at the depth of interest. Even though salt dissolves with time and produces brine, the shape of the salt layer does not change. In their study, Ranganathan and Hanor (1988) made a similar assumption for salt domes.
- At the basement a constant temperature boundary condition is defined. The value is set to 150 °C which corresponds to a linear vertical gradient of 30 °C/km.
- The lateral boundaries are closed to fluid, heat, and mass flow.

The simulation of transient flow requires a priori knowledge of physically meaningful initial conditions, which can be obtained from a steady-state calculation of the problem or from the interpolation of observed data. Initial conditions derived from observed data introduce perturbations to the parameters field which immediately initializes high numerical instabilities. Therefore the numerical system will need a large number of time steps for calculating the solution and in some cases will not converge at all.

On the other hand, using initial conditions derived from steady-state solutions of the considered problem guarantees a higher stability of the simulations and increases the rate of convergence of the coupled equations (Ortega and Rheinboldt 1970). Nevertheless, obtaining steady state solutions for coupled nonlinear systems as in the thermo-convective case is in most cases impossible. Therefore, the initial pressure and temperature distributions are obtained from the numerical solution of uncoupled steady-state fluid flow and heat transport models. The resulting pressure profile is not disturbed, it is hydrostatic. In order to calculate the initial temperature distribution, the hydraulic conductivity value of each layer has been set close to 0. Therefore the resulting temperature profile is purely conductive. The initial temperature field prescribed for the thermohaline simulations is illustrated in Fig. 2-3B. For presentation, the temperature values have been interpolated with a Kriging gridding method by use of the commercial software Surfer 8. This figure illustrates the well-know thermal anomalies around salt domes. Concave isothermal lines are associated with the salt domes whereas above these structures the isothermal lines are convex. Such anomalies are due to the high thermal conductivity of the salt domes with regard to the thermal conductivity of the surrounding sediments.

The initial salt concentration is homogenous and set to fresh water condition (0 g/L) everywhere above the Top Salt.

2.2.3. Numerical and time step schemes

As mentioned in paragraph 2.1.1, the physical perturbations which arise during the simulation of thermohaline flow are caused by heterogeneous physical parameters which are encountered in all hydrothermal systems. Additionally, strong buoyancy forces together with steep gradients dramatically trigger the numerical instabilities of the system. These instabilities, also referred to as wiggles, are manifested by negative values of nonnegative properties such as fluid density or concentration. Wiggles have a numerical nature. They signal that the gradients are insufficiently resolved by the mesh. As a result, numerical errors are generated. In density plume problems the perturbations created by the propagation of these numerical errors are virtually uncontrollable (Schincariol et al. 1994). To prevent such wiggles an extremely refined mesh is required. Unfortunately, such a grid resolution cannot be achieved at the basin-scale ($1x10^2$ km) with regard to the computational power of the available software and hardware. The numerical compromise is the use of a full upwind scheme. This

numerical scheme introduces a balancing tensor diffusivity term to stabilize the solution. This is equivalent to an increase the coefficient of molecular diffusivity $\mathbf{D}_{\mathbf{diff}}$ appearing in Eq.(2.3) according to Diersch and Kolditz (2002):

$$\mathbf{D}^{\mathrm{num}} = \mathbf{D}_{\mathrm{diff}} + \frac{v\Delta l}{2} + o(\Delta l^2)\,, \tag{2.7}$$

where v is the fluid pore velocity and Δl the characteristic element length. Such numerical diffusion (or artificial dissipation) is represented by the second term in the right hand side of Eq.(2.7), $\frac{v\Delta l}{2}$. From this relation, it can be inferred that the physics of the problem is highly changed if a too coarse mesh (i.e., large Δl) is used. At large Δl an overestimated numerical diffusion will be introduced and will govern the whole transport process. Therefore the resulting over-dispersive smoothing will overwhelm thermally buoyant induced flow. Consequently no temperature effects on the flow regime can be taken into account. Particular attention must be made in defining a correct space gridding that prevents the upwinding scheme to introduce dominant over-dissipative terms.

Transient simulation of convective processes also requires proper time schemes. Here a predictor-corrector time integrator (Gresho and Sani 2000) advances the balance equations in time. Specifically, the second order Trapezoid Rule scheme (TR) with automatically controlled time-stepping is used. This scheme has been proved to be an accurate strategy especially for strong nonlinearities (Diersch and Kolditz 1998). At each time step a convergence tolerance factor directly controls the time-step size. If the error estimates do not violate the constraints, the time step is increased, otherwise the time-step is reduced. Fig.2-4 illustrates the adaptive time scheme strategy. More details about this temporal discretization can be found in the WASY white papers (WASY-GmbH 2002).

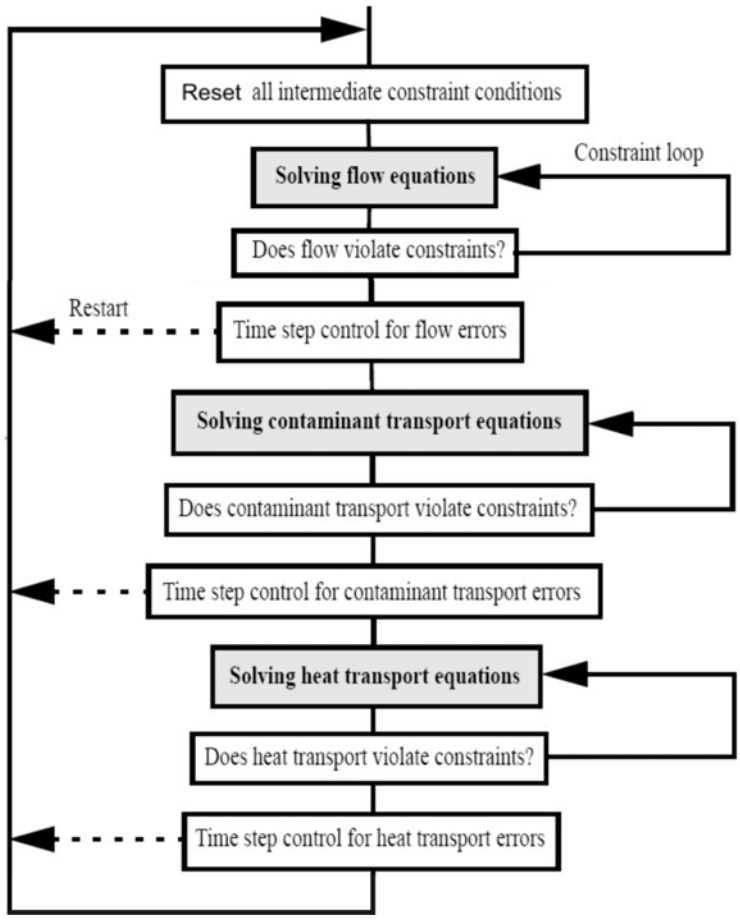

Fig.2-4: Adaptive time scheme strategy for coupled transient flow, mass and heat transport.(Modified from Diersch and Kolditz 1998).

In order to gain insights into the temporal evolution of the studied system a reasonable computing time interval has to be set. For the problem considered here, such an interval is strictly artificial, having no relation to any geological timescale. Nevertheless, the computing time interval should not be too low with regard to the geological time-range of flow processes in sedimentary basin (i.e. ka or Ma). Here a computing time interval of 200 ka has been set. When a time scale will be mentioned in the description of the results, it will be referred to computing time with no regard to a particular geological timescale.

In bad-posed problems the predicted time-step size decreases asymptotically at a certain moment of the numerical simulation process. Consequently the numerical problem cannot be solved within the appointed computing time interval. During the iterative process this behaviour indicates that the constraints cannot be satisfied. This is likely due to an insufficient mesh definition. In other words, the finite elements of the grid simply do not work.

2.2.4. Building a mesh suitable for the thermohaline approach

According to the previous considerations, a mesh suitable for thermohaline flow can be defined. The finite element composing the mesh should be constructed so that an asymptotic decrease of the time-step will not arise. The iterative time scheme will then run over the prescribed computing time-scale (200 ka) and a preliminary solution of the transient problem can be obtained. Moreover temperature effects on the flow regime must be taken into account. Therefore the mesh must be sufficiently refined in order to avoid over-dissipative terms introduced by the upwinding scheme (Eq.(2.7)). The last requirement is that mesh convergence is achieved. This implies that further refinement of the spatial discretizations will not introduce discrepancies in the results, i.e. the numerical calculations are independent from additional mesh refinements.

Fig 2-5 illustrates the finite element mesh of the representative cross-section obtained from the integrated 3D structural model. For pictorial needs a 10:1 vertical exaggeration is used. The mesh density is derived by the original resolution of the structural model.

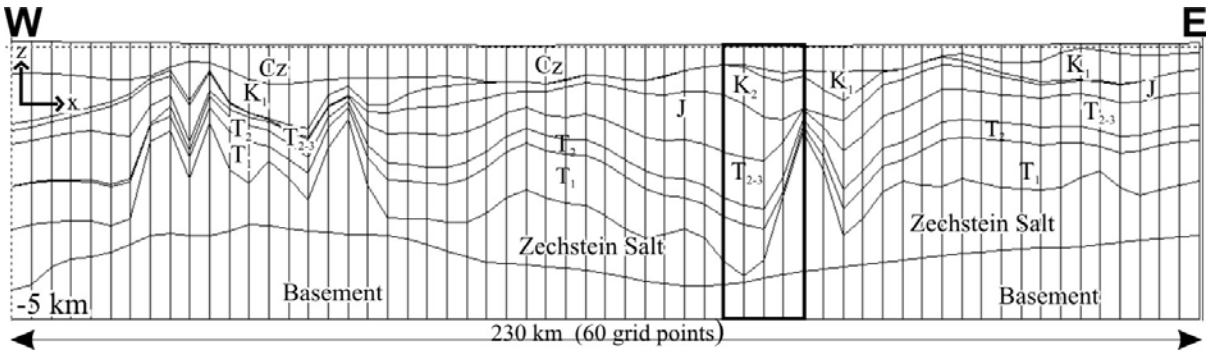

Fig.2-5: Initial finite element mesh obtained from the original 3D structural model of the NEGB. For pictorial needs a 10:1 vertical exaggeration is used. 60 grid points discretize each model slices. The rectangle delimits a salt dome environment which is illustrated in Fig.2-6 and Fig.2-7 with no vertical exaggeration.

As mentioned in paragraph 2.1.2. each model slice is discretized by 60 nodes and every layer is composed of 59 quadrilateral elements. The mesh resolution is 3.9 km in the horizontal direction (**x**). The vertical mesh resolution is determined by the layer thickness and can span from few meters up to 1 km. The morphology of all stratigraphic units in the neighbouring of salt diapirs is highly deformed. The finite elements geometry is extremely distorted especially in the vertical direction (**z**). The elements taper at the salt dome crests, i.e. the quadrilaterals are narrow trapezoids.

It turned out that the time-step size decreased asymptotically when this finite element mesh was used to solve the thermohaline problem. Moreover this problem arose as soon as

the simulation was initialized. Therefore the simulated computing time could not cover 200 ka.

All 2D finite elements are formulated such that a perfect equilateral triangle or square give the best answers. As elements deviate from these perfect shapes, there is a corresponding degradation in the computed results (MacNeal 1990). The element aspect ratio is an helpful indicator of the element performance. This ratio is defined as the value obtained by dividing the maximum length of the element in the horizontal direction (**x**) by the maximum length in the vertical direction (**z**). Square mesh elements are associated to unitary aspect ratio. At the resolution of 60 grid points per slices all elements discretizing the model area present an aspect ratio higher than one, i.e. the quadrilaterals are elongated in the horizontal direction (**x**). A mesh refinement applied in the vertical direction (**z**) increases the density of nodes in the **x** direction. Consequently, vertical refinements can lead to an element aspect ratio value close to one. Fig. 2-6 illustrates a zoom of the finite element discretizing a salt dome. No vertical exaggeration is used.

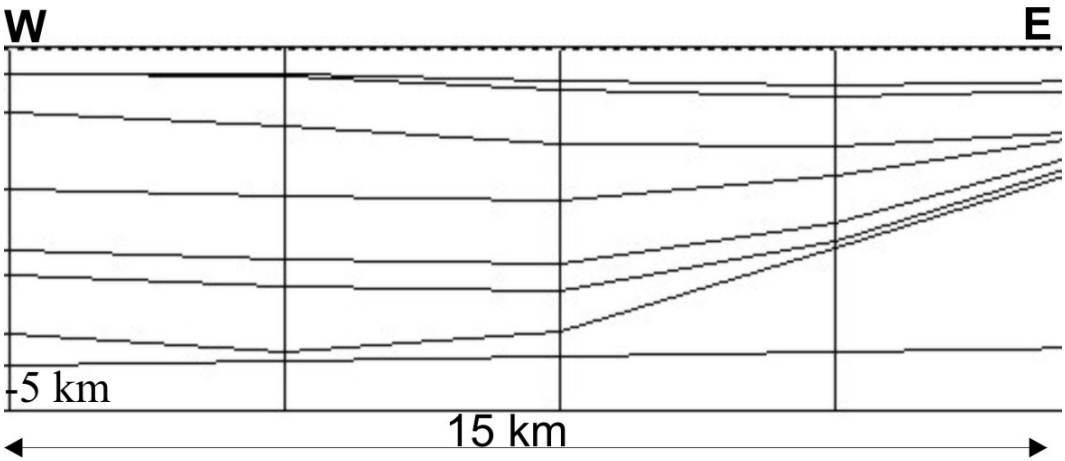

Fig.2-6: Zoom of the initial finite element mesh in salt a dome environment. No vertical exaggeration. The mesh resolution of the cross-section from which this zoom is obtained is 60 grid points per slice. The chosen salt dome is localized in the rectangle depicted in Fig.2-5.

The finite elements taper along the steep salt flanks. No vertical refinement can possibly transform these distorted elements to squares. Since many salt domes are included in the domain, perfect square elements cannot be obtained throughout the whole model area. A compromise has to be found. In this context, the only way to obtain “good” elements that will work for the simulation process, is to apply a vertical refinement on the whole mesh and test whether the simulation based on this denser mesh can run over the appointed computing-time or not. If an asymptotical decrease of the time-step occurs during the simulation it is probably because most of the elements do not work properly. A denser vertical refinement is then

necessary. Eventually a correct mesh discretization is obtained by repeatedly applying the described procedure. The refinement can be easily applied on the original structural model by the use of the FEFLOW mesh editor interface. This pragmatic approach can hopefully be successful in building a robust finite element mesh suitable for thermohaline problem. If so, the simulation will run over the computing time interval and a preliminary "solution" can be achieved.

Fig.2-7 is a sketch illustrating the mesh robustness as a function of the number of grid points discretizing the model slices. The robustness index is "0" when asymptotical decrease of the time-step has occurred during the simulation and the calculations could not be completed. "1" indicates that the simulation ran successfully over the computing time interval of 200 ka. Vertical refinements have been applied up to 200 nodes per slices. It can be seen that a successful simulation has been carried out on a mesh having 159 grid points per slices. An interesting feature of the mesh robustness can be inferred by from Fig.2-7.

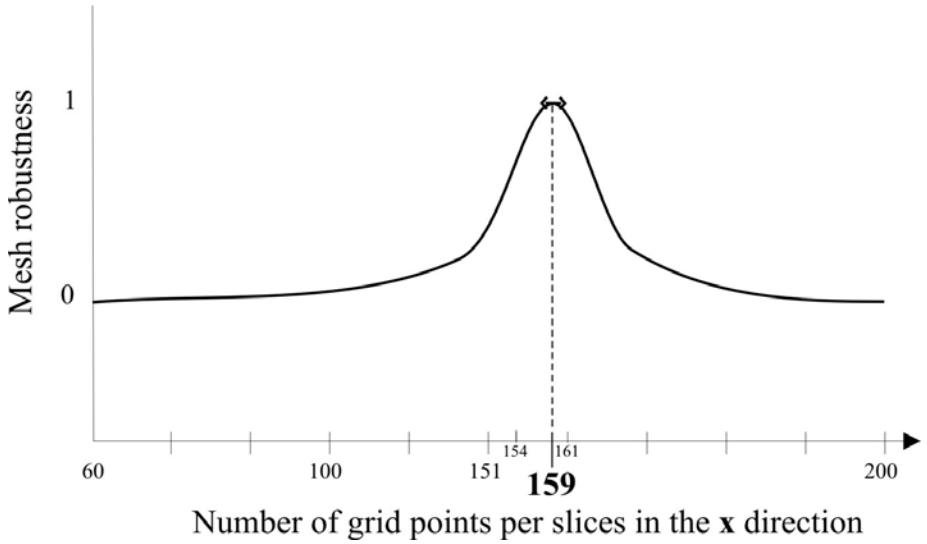

Fig. 2-7: Sketch illustrating the mesh robustness as a function of the number of grid points discretizing the model slices in the horizontal direction (**x**).

The simulation process is very sensitive to the number of grid points discretizing the slices. As long as this number is far from 159 the simulations could not be completed: numerical oscillations occurred immediately after the process was initialized and the predicted time-step decreased asymptotically. On the other hand, simulations based on meshes having a grid density very close to 159 points per slices could run over 200 ka although with some time-step oscillations. Higher vertical mesh refinements did not improve the simulation stability, in contrary it is declining.

Fig.2-8 illustrates the resulting refined finite element mesh in a salt dome environment (cf. Fig.2-6) No pictorial vertical exaggeration is used. The thicker quadrilaterals are less elongated and are slightly close to square shape in some distance from the salt flanks.

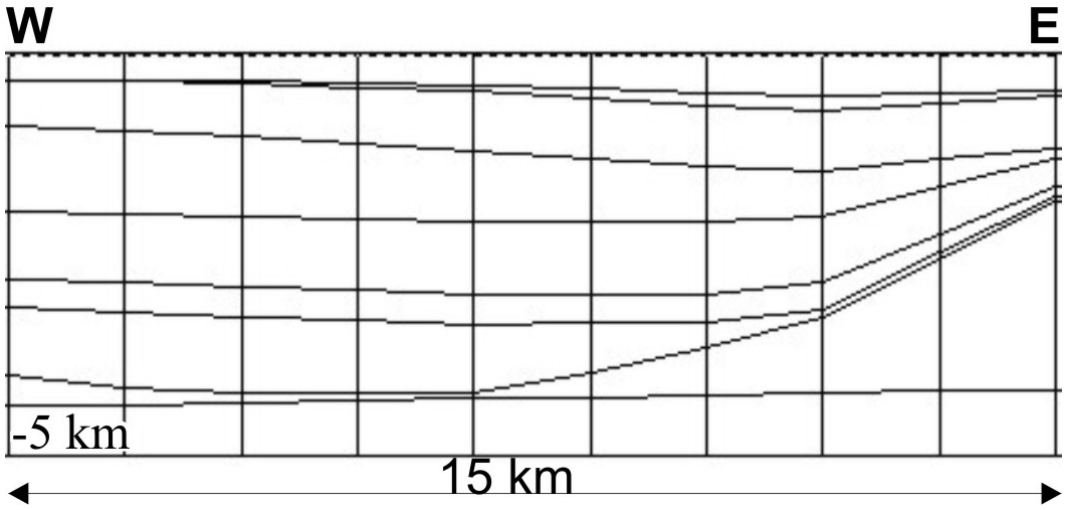

Fig.2-8: Zoom of the refined finite element mesh in salt a dome environment. No vertical exaggeration. The mesh resolution of the cross-section from which this zoom is obtained is 159 grid points per slice. The chosen salt dome is localized in the rectangle depicted in Fig.2-5.

At this point a mesh allowing a complete simulation run over the computing time (200 ka) has been obtained. Longer term calculations have been successfully performed on this mesh up to 400 ka. The whole model area is now composed of 1422 elements, each slice being discretized by 158 nodes. This value corresponds to a mesh resolution of 1.45 km in the horizontal direction. However, numerical dissipative terms introduced by the upwind balancing tensor diffusivity (Eq.(2.7) can still be dominant at this mesh resolution. If this is the case, only the numerical diffusivity governs the transport process. As a result, thermohaline and coupled fluid flow-mass transport simulations lead to the same mass profile. In order to check whether this is the case or not the mass profile resulting from a coupled fluid flow-mass transport problem has been compared to the mass profile obtained from a thermohaline simulation. The results are illustrated in Fig.2-9.

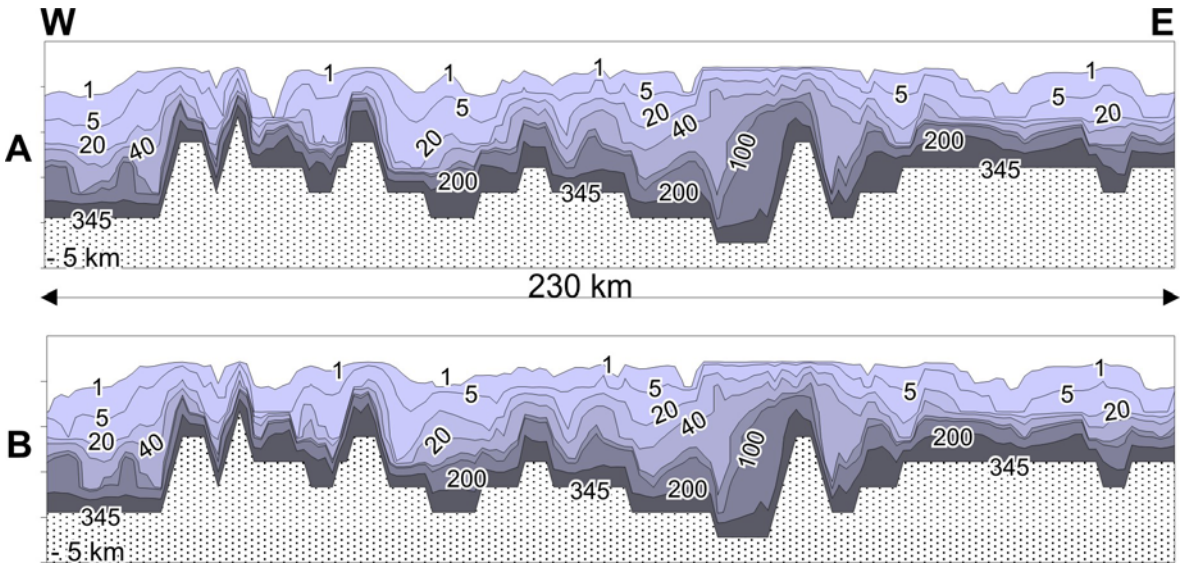

Fig.2-9: Mass distribution obtained from: a thermohaline simulation (**A**), and from a coupled fluid flow and mass transport simulation (**B**).

No significant variation can be observed by comparing the mass distribution obtained from thermohaline simulation (Fig.2-9A) with the mass distribution derived from a coupled fluid flow and mass transport problem (Fig. 2-9B). The transport process is dominated by the over-estimated numerical dissipation and the resulting mass profile has no physical meaning. Temperature effects on solute transport are overwhelmed and cannot be taken into account at this mesh resolution. The actual mesh is surely robust, providing a "solution" of the problem. Nevertheless, robustness alone is not sufficient. Indeed the solution is only mathematically correct but physically unlikely. At this mesh resolution, the numerical scheme defines a problem which is completely different from the real natural system. Therefore the mesh has to be further refined.

In order to preserve the global aspect ratio of the finite elements, which has until now ensured the mesh robustness, vertical and horizontal mesh refinements are performed simultaneously. In this way, an element will be subdivided in 4 new elements having the aspect ratio of the original element. This refinement procedure has been repeatedly applied until both thermohaline and coupled fluid flow-mass transport simulations have provided different mass patterns. It turned out that two consecutive refinements were necessary in order to observe substantial differences in the mass profiles of the two different problems. Each finite element is therefore subdivided in 16 new elements. The whole model consists of 22752 elements (1422 x 16). The total number of slices is 37, each of them being discretized by 633 nodes. The mesh resolution is 364 m in the horizontal direction (**x**). Fig.2-10 illustrates the resulting mesh in a salt dome environment. At this resolution, temperature effects on the

transport process can be taken into account. The simulation results based on this refined mesh will be shown in the next chapter.

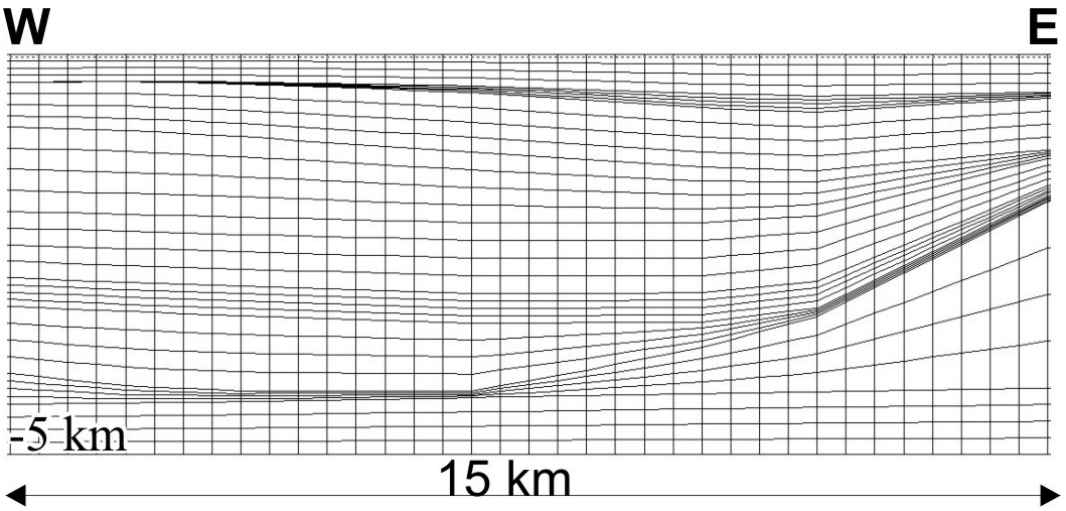

Fig.2-10: Zoom of the final finite element mesh in salt a dome environment. No vertical exaggeration. The final mesh resolution of the cross-section from which this zoom is obtained is 633 grid points per slice. The chosen salt dome is localized in the rectangle depicted in Fig.2-5.

With the purpose of testing the grid convergence an additional refinement has been applied. No spatial discretization effects were observed with regard to the mass patterns of the thermohaline problem. The results are independent from further mesh refinements. This proves that the actual resolution the finite element mesh ensures convergence.

2.3. Discussion

In this chapter a representative cross-section of the NEBG has been obtained. The initial mesh resolution of the original structural model has been refined so that:

- A preliminary solution can be calculated over a prescribed computational time of 200 ka, or even longer.
- The numerical scheme approximations do not dominate the transport processes. Brine flow induced by concentration and temperature gradients can be taken into account by the mesh.
- The grid convergence is achieved.

The final mesh consists of 23421 nodes (22752 elements) with a resolution of 364 m in the horizontal direction.

Fluid flow, heat and mass transport simulations will be henceforth based on this finite element mesh. In the next chapter the mechanisms driving salt within the NEGB will be investigated. A new set of boundary conditions will be defined in order to reproduce observed data such as brine and fluid temperature distribution at the surface. The interaction between topography driven flow and solute transport will be quantified (forced versus free convection). The main fluid-dynamics of salt migration throughout the sediments fill will be inferred from evolution analysis of the transport processes. Furthermore, viscosity effects will be taken into account and evaluated. Based on these 2D numerical results, a regional picture of the transport processes affecting the NEGB will be tracked down.